Catalysis Today xxx (xxxx) xxx

Contents lists available at ScienceDirect

Catalysis Today

journal homepage: www.elsevier.com/locate/cattod

Improved photocatalytic activity of SnO_2-TiO_2 nanocomposite thin films prepared by low-temperature sol-gel method

Ksenija Maver [a], Iztok Arčon [a,b,*], Mattia Fanetti [a], Samar Al Jitan [c,d], Giovanni Palmisano [c,d], Matjaž Valant [a,e], Urška Lavrenčič Štangar [f,**]

[a] University of Nova Gorica, Vipavska 13, SI-5000 Nova Gorica, Slovenia
[b] Jožef Stefan Institute, Jamova 39, SI-1000 Ljubljana, Slovenia
[c] Department of Chemical Engineering, Khalifa University of Science and Technology, P.O. Box 127788, Abu Dhabi, United Arab Emirates
[d] Research and Innovation Center on CO2 and H2, Khalifa University of Science and Technology, P.O. Box 127788, Abu Dhabi, United Arab Emirates
[e] Institute of Fundamental and Frontier Sciences, University of Electronic Science and Technology of China, Chengdu 610054, China
[f] University of Ljubljana, Faculty of Chemistry and Chemical Technology, Večna pot 113, SI-1000 Ljubljana, Slovenia

ARTICLE INFO

Keywords:
SnO_2-modified TiO_2
Photocatalytic activity
Low-temperature
Thin films
XAS analysis

ABSTRACT

The objective of this research was to investigate how the photocatalytic activity of pure TiO_2 can be improved by SnO_2 modification. Different molar ratios of tin to titanium were prepared. The correlation between tin concentration and structural properties was investigated to explain the mechanism of photocatalytic efficiency and to optimize the synthesis conditions to obtain enhanced activity of the SnO_2-modified TiO_2 photocatalysts under UV-irradiation. The SnO_2-modified TiO_2 photocatalysts were prepared by a low-temperature sol-gel method based on organic tin and titanium precursors. The precursors underwent sol-gel reactions separately to form SnO_2-TiO_2 sol. The sol-gels were deposited on a glass substrate by a dip-coating technique and dried at 150 °C to obtain the photocatalysts in the form of a thin film. To test the thermal stability of the material, an additional set of photocatalysts was prepared by calcining the dried samples in air at 500 °C. The photocatalytic activity of the samples was determined by measuring the degradation rate of an azo dye. An increase of up to 30% in the photocatalytic activity of the air-dried samples was obtained when the TiO_2 was modified with the SnO_2 in a concentration range of 0.1–1 mol.%. At higher SnO_2 loadings, the photocatalytic activity of the photocatalyst was reduced compared to the unmodified TiO_2. The calcined samples showed an overall reduced photocatalytic activity compared to the air-dried samples. Various characterization techniques (UV-Vis, XRD, N_2-physisorption, TEM, EDX, SEM, XAS and photoelectrochemical characterization) were used to explain the mechanism for the enhanced and hindered photocatalytic performances of the SnO_2-modified TiO_2 photocatalysts. The results showed that the nanocrystalline cassiterite SnO_2 is attached to the TiO_2 nanocrystallites through the Sn-O-Ti bonds. In this way, the coupling of two semiconductors, SnO_2 and TiO_2, was demonstrated. Compared to single-phase photocatalysts, the coupling of semiconductors has a beneficial effect on the separation of charge carriers, which prolongs their lifetime for accessibility to participate in the redox reactions. The maximum increase in activity of the thin films was achieved in the low concentration range (0.1–1 mol.%), which means that an optimal ratio and contact of the two phases is achieved for the given physical parameters such as particle size, shape and specific surface area of the catalyst.

1. Introduction

In photocatalysis, the positions of the energy levels of the band gap of a semiconductor determine the chemical potentials of the photogenerated electrons and holes to participate in redox reactions [1]. In this respect, TiO_2 has particular electronic structure as it allows simultaneously the oxidation of hydrogen and the reduction of oxygen. TiO_2 is the most widely used among the other semiconductors. Besides, TiO_2 also has other advantageous physiochemical properties such as availability, low cost, biocompatibility, chemical stability and corrosion

* Corresponding author at: University of Nova Gorica, Vipavska 13, SI-5000 Nova Gorica, Slovenia.
** Corresponding author.
E-mail addresses: iztok.arcon@ung.si (I. Arčon), urska.lavrencic.stangar@fkkt.uni-lj.si (U. Lavrenčič Štangar).

https://doi.org/10.1016/j.cattod.2021.06.018
Received 3 April 2021; Received in revised form 2 June 2021; Accepted 23 June 2021
Available online 25 June 2021

resistance [2]. For these reasons, titanium dioxide is used in numerous applications: water purification, degradation of air pollutants, removal of pesticide residues, self-cleaning coatings, dye-sensitized solar cells, water splitting, etc. However, there is a continuous search for novel, more efficient photocatalysts with improved beneficial properties or avoiding their weaknesses.

One of the drawbacks of TiO_2 photocatalyst is high electron-hole recombination rate [3,4] and coupling with other semiconductors is one of the strategies to improve its efficiency. It has been shown that a mixture of anatase and a small percentage of rutile phase improves the photoefficiency compared to anatase phase alone, although it is considered the most efficient among TiO_2 phases [2]. This approach is successfully applied in the benchmark TiO_2 photocatalyst Degussa P25 (Evonik) [5,6]. Since cations of some elements, such as Sn, promote the conversion of anatase to rutile at much lower temperatures compared to undoped TiO_2 [7], these cations can be used as promoters to induce an anatase/rutile coupled system with enhanced photoactivity [8].

When low concentrations of Sn are used to modify TiO_2, the conversion of anatase to rutile is the energetically preferred situation [8–12]. At higher Sn contents (above 10 mol.%), the surface segregation of SnO_x clusters has often been observed [8,11]. Tin in the form of oxide, SnO_2, has been successfully used in coupled systems with TiO_2 in spite its wide band gap (3.8 eV) [13–16]. In both cases, either by doping TiO_2 with Sn ions or by forming a composite with SnO_2, a coupled system of two semiconductors with enhanced photoactivity is formed.

Two semiconductors with different band gaps enhance the photogenerated charge carrier separation as long as the relative energies of the bands and the contact between the components are sufficient [2]. In this way, electrons migrate from the higher energy conduction band to the lower energy one, while holes migrate from the lower valence band to the higher energy one. The physical separation of the charges reduces the recombination rate and thus improves the photocatalytic performance by increasing the lifetime of the charge carriers. In the case of TiO_2/SnO_2 diphase system, the relative energy position of the bands and the process of charge carrier separation is schematically depicted in Fig. 1.

In addition to the width of the band gap and its position relative to the energy levels of various redox potentials, there are other factors, such as crystallite size, morphology and surface area, that characterize an efficient photocatalyst [2]. And for any composite system, an optimum ratio of two phases is expected to achieve maximum photocatalytic performance. However, this ratio strongly depends on the extent of contact between the different phases and thus on the preparation method. For this purpose, an optimal ratio between the two phases has to be determined to obtain sufficient bonding of two semiconductors.

In most reported synthesis methods, inorganic salts $SnCl_2$ or $SnCl_4$ are used as Sn source [13–17] which requires high temperatures to remove chlorine ions from the solution. Very rarely, Sn alkoxides are used as the starting material [18–20]. In this study, we used organic Ti- and Sn-tetraisopropoxide and a sol-gel synthesis route to prepare high-purity materials at low temperatures. Low-temperature treatment

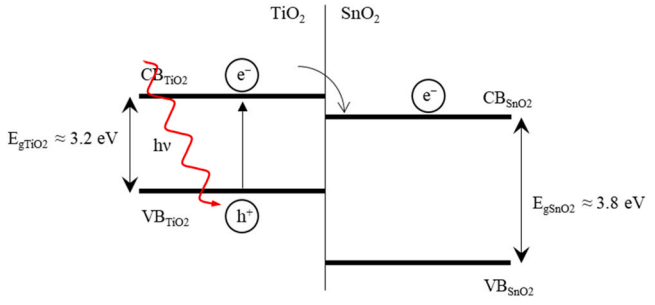

Fig. 1. Relative energy position of the bands and the process of charge separation in the TiO_2/SnO_2 system.

of the films was used to make the coatings potentially even more applicable, for example, on the inbuilt surfaces or on substrates that are thermosensitive.

In our previous work [8], we have improved the photocatalytic properties of TiO_2 by incorporating Sn cations into the TiO_2 crystal structure of titania nanoparticles. In this work, we report about a TiO_2-SnO_2 coupled system of two semiconductors with enhanced photoactivity. We achieved the formation of a mixed system by a sol-gel synthesis route in which the Ti and Sn precursors underwent the condensation and hydrolysis processes separately. The sols were additionally mixed together and then deposited on the glass substrates by a dip-coating technique to obtain thin films. After drying (at 150 °C), the films show an improved photoactivity compared to unmodified TiO_2, implying that the active phases are already achieved during the formation of the sols. To the best of our knowledge, this is the first report of evidence for the coupling of two semiconductors, SnO_2 and TiO_2, at the atomic level at the low temperature synthesis conditions with boosted photocatalytic activity of transparent thin films. We found that in the low concentration range of SnO_2 (below 1 mol.%), an optimal ratio between titania and cassiterite phases is obtained, which facilitates charge separation and enhances the photocatalytic efficiency of SnO_2--modified titania films compared to unmodified one.

2. Materials and methods

2.1. Preparation of photocatalysts

Adapting our previously proposed synthesis route [8], we have separately prepared unmodified TiO_2 and SnO_2 sol by using titanium(IV) isopropoxide (TiTIP, 97%, from Aldrich) as a source of titanium and tin (IV) isopropoxide (SnTIP, 10 wt%, from Alfa Aesar) as a source of tin. The selected precursors were stirred with ethanol absolute (from Carlo Erba) in equal molar ratios. Acidic water, 0.25 M HNO_3, was prepared separately (from concentrated nitric acid (70%, from Acros Organics) and double deionized water by a NANOpure system, Barnstead) in the amount of 100-time molar excess to metal and added to metal alkoxide solution dropwise under vigorous stirring to disperse the hydrolysed drops homogeneously. The hydrolysis of metal alkoxides resulted in the formation of amorphous white precipitates. After refluxing for 48 h at 85 °C, a stable milky white (in the case of TiO_2) or yellowish (in the case of SnO_2) sols were obtained. In the next step, both TiO_2 and SnO_2 sols were stirred together for 1 h at ambient temperatures in different Sn: Ti ratios, marked as $x$$SnO_2$-$TiO_2$, where x denotes the relative amount of Sn in mol.%. Five different SnO_2 concentrations were selected (0.05; 0.1; 0.5; 1 and 10 mol.%).

Unmodified and SnO_2-modified titania thin films (thickness of about 150 nm) were deposited on both sides of microscopic glass slides (LLG Labware, 70 mm × 12.5 mm × 1 mm) by a dip-coating method. The substrate was dipped into the sol at room temperature and withdrawn at the speed of 10 cm/min. The coated films were dried at room temperature and then heated at 150 °C for 2 h. In addition, another set of coatings were prepared by further calcination at 500 °C in air for 2 h. All films obtained in this work are transparent over the whole visible spectral range, as demonstrated by UV–vis transmittance spectra (Fig. S1 in Supplementary Materials), and uniform (SEM image in Fig. S2a in Supplementary Materials). The thickness of a single layer is 110–150 nm (SEM image in Fig. S2b in Supplementary Materials).

The sample powders of the photocatalysts were prepared by scratching off the films from the glass substrates, followed by grinding in a mortar.

2.2. Characterization methods

The photocatalytic efficiency of the thin films was determined by measuring the degradation rate of azo dye plasmocorinth B (PB, 60% from Sigma Aldrich, initial concentration of 12 mg/l). The experiment

was performed in a home-made photoreactor [21] with six UV-lamps (Blacklight Blue, 36 W/m^2) placed around the central cell. The cell consisted of eight glass slides covered with one layer of photocatalyst on both sides of the glass (total film-liquid surface area of 96 cm^2). The PB solution was purged with oxygen (flow rate of 100 ml/min) to additionally enhance oxidative mineralization of the dye. Dye concentration decrease upon UV-irradiation time was determined spectrophotometrically (Agilent Cary 60 UV–vis Spectrophotometer, λ = 400–800 nm) by monitoring the dye absorbance maximum ($\lambda_{max} \approx 527$ nm), converted to concentration using Beer-Lambert law [22], $A = \varepsilon \cdot l \cdot c$, where A is the absorbance of the PB solution at 527 nm excitation at different illumination times, c is the molar concentration of PB at different illumination times, ε is the molar absorptivity coefficient (36,126 l mol^{-1} cm^{-1} for PB) and l is the optical path length. Dye discoloration is a degradation process [23], described as first-order reaction kinetics [21], $c/c_0 = e^{-k1 \cdot t}$, where k_1 is a first-order rate constant and used for the numerical evaluation of photoefficiencies of the catalysts. At the initial times the dye degradation can be approximated by linear function ($c/c_0 \approx 1 - k_1 \cdot t$). For all the samples, unmodified and SnO_2-modified photocatalysts, the effect of dye adsorption process was separated from the effect of photocatalytic degradation of the dye by starting the UV-illumination of the cell after there was no decrease of dye concentration in the dark detectable (approximately after 30 min). A prolonged measurement was carried out in the dark conditions on the unmodified TiO_2 photocatalysts dried at 150 °C to prove that there is no decrease of PB dye concentration over irradiation time due to adsorption. The result is presented in Fig. 3a as grey squares. Moreover, the degradation of PB itself under UV can be excluded [24].

As a reference, the photoactivity of the commercially available SGG Bioclean® glass was measured in the same reactor and under the same conditions with the same geometric area exposed to UV irradiation. The photodegradation rate constant k_1 was determined and compared with the unmodified TiO_2 sample dried at 150 °C. The result is shown in the histogram in Fig. 3b and in Table S3 (in Supplementary Materials).

For comparison, the photoactivity of the unmodified TiO_2 sample dried at 150 °C in simulated waste water was also measured (detailed composition is described in Supplementary Materials in Table S4). The photodegradation rate constant k_1 was determined and compared with the k_1 constant obtained from the experiments with the azo-dye dissolved in deionized water. The result is shown in Table S3 (in Supplementary Materials).

The repeatability of the photocatalytic experiment (further information in the Supplementary Materials in Section 2.1) was tested by repeating the entire experiment under the same conditions. For this purpose, three sets of unmodified TiO_2 photocatalysts dried at 150 °C were prepared in the form of thin films and stored in the dark. The constant rates k_1 in the photodegradation experiments can be determined with a relative accuracy of 1%.

The reusability of the photocatalysts (further information in Supplementary Materials in Section 2.2) was tested by repeating the photocatalytic experiment three times with the same set of photocatalyst (Sn-modified TiO_2 with 0.5 mol.% Sn, dried at 150 °C). Between the repetition, the glass slides coated with the photocatalyst were washed with deionized water and placed in the UV-chamber for 5 h to clean up any possible residue products adsorbed on the surface from previous photodegradation experiments. The photodegradation rates of the reused samples differ within 5%, indicating that the adhesion of the films, although heated only to 150 °C, is good enough to be reused.

The crystalline structure of the photocatalyst powders was analysed by X-ray diffraction (XRD) patterns taken with Rigaku Mini Flex 600 powder diffractometer in reflection mode using Cu Kα irradiation. The quantitative phase composition analysis and evaluation of the lattice parameters were performed by Rietveld refinement method using PANalytical X'Pert High Score Plus software [25]. The crystallite size was determined by the Scherrer formula [26]: $d = 0.9\lambda/(\beta \cos\theta)$, where d is the crystallite size in nm, λ is the wavelength of X-ray in Å (1.5418 Å), β is the full width of diffraction peaks at half maxima (FWHM) in radians, and θ is the Bragg angle. Diffraction peaks of the (101) anatase, (121) brookite and (110) rutile for titania and (110) for cassiterite SnO_2 were used to evaluate the crystallite size. JCPDS databases 96-900-9087 for anatase, 96-900-4139 for brookite, 96-900-4145 for rutile TiO_2 and 96-210-4755 for cassiterite SnO_2 were used for the peaks identification.

The BET specific surface area of the photocatalyst samples in powder form was evaluated from N_2 sorption isotherms obtained at 77 K using a Tristar 3000 Micromeritics volumetric adsorption analyser. The BET specific surface area was calculated from adsorption data in a relative pressure range from 0.01 to 0.95 [27]. The pore size distributions were calculated from nitrogen adsorption data using the Barrett-Joyner-Halenda method [28].

The electron microscopy analysis was performed by field-emission transmission electron microscope (JEM-2100F, JEOL) operated at 200 kV. The microscope is equipped with a scanning transmission electron microscopy (STEM) unit and a detector for energy-dispersive X-ray (EDX) mapping and spectroscopy (X-MAX80T, Oxford). The samples were prepared by immersing a Lacey-carbon TEM grid in a water suspension of photocatalyst powders and air-dried at room temperature. The images were analysed using ImageJ 1.52a software [29].

The morphology and thickness of thin films was examined using a field emission scanning electron microscope (Ultra Plus Zeiss), using a primary electron voltage of 20.0 keV. Selected sample photocatalysts were deposited on a silicon wafer in one layer by dip-coating at the speed of 10 cm/min and dried at 150 °C for 2 h.

The local atomic structure around Sn cations in the SnO_2-modified titania and reference SnO_2 photocatalysts was analysed by X-ray absorption spectroscopy. Sn K-edge EXAFS (Extended X-ray Absorption Fine Structure) spectra of the samples were recorded at room temperature in the transmission detection mode at the P65 beamline of PETRA III, DESY, Hamburg, Germany. The powders of SnO_2-modified titania photocatalyst and crystalline SnO_2 reference sample (Sigma Aldrich) were prepared as self-supporting homogenous pellets with total absorption thickness (μd) about 2 above the Sn K-edge. A Si (311) crystal monochromator was used with energy resolution of about 3 eV at the Sn K-edge (29,200 eV). Higher-order harmonics were removed by a flat Pt coated mirror placed in front of the monochromator. The intensity of the monochromatic X-ray beam was measured by three consecutive ionization detectors (5 cm long ionisation chambers; the first filled with 400 mbar Kr and 600 mbar N_2, the second and the third with 1000 mbar Kr). The samples were mounted on the sample holder placed between the first and second ionization detector. The absorption spectra were measured in the energy region from −150 eV to +1000 eV relative to the Sn K-edge. In the edge region equidistant energy steps of 0.25 eV were used, while in the EXAFS region equidistant k steps of 0.03 Å^{-1} were collected. Up to three repetitions of the scans with integration time of 0.2 s/step were superimposed to improve signal-to-noise ratio. The exact energy calibration was established with simultaneous absorption measurement on a 20-micron thick Sn metal foil placed between the second and the third ionization chamber. Absolute energy reproducibility of the measured spectra was ±0.03 eV. The quantitative analyses of EXAFS spectra were performed with the IFEFFIT program package [30]. Structural parameters of the EXAFS spectra were quantitatively resolved by comparing the measured signal with the model, constructed with the FEFF6 program code [31], in which the photoelectron scattering paths are calculated ab initio from a tentative spatial distribution of neighbour atoms.

Photoelectrochemical measurements were carried out as previously described in [32] using a Metrohm Autolab PGSTAT302N Potentiostat in a standard three-electrode cell with the sample deposited on fluorine doped tin oxide (FTO) as the working electrode, platinum electrode as the counter electrode, and Ag/AgCl electrode as the reference electrode. The electrolyte solution was 0.5 M Na_2SO_4. Photocurrent transients were recorded at a potential of 0.6 V vs Ag/AgCl electrode.

Electrochemical impedance spectroscopy (EIS) was performed in dark and under UV–vis illumination in the frequency range of 0.1 Hz–10 kHz with an applied potential of 0.6 V vs Ag/AgCl electrode. Mott-Schottky experiments were conducted with a potential step of 50 mV at a constant frequency of 10 kHz. A 50 W light-emitting diode source with an emission centered at 382 nm was used for irradiation. The average values of the radiation reaching the sample surface, measured with a DeltaOhm 9721 radiometer and matching probes, were 52.8 and 41.6 W/m^2 in the 315–400 and 450–950 nm ranges, respectively.

A schematic diagram of the photocatalyst preparation and characterization is presented in Fig. 2.

3. Results and discussion

3.1. Photocatalytic activity results

The photocatalytic activity of the photocatalysts in the form of thin films was determined by measuring the degradation of PB dye as a function of UV-irradiation time. The degradation of PB dye as a function of UV-illumination time for unmodified TiO_2 and SnO_2-modified TiO_2 film catalysts with different SnO_2 concentrations (0.05–10 mol.%) and pure SnO_2 catalyst (obtained from SnO_2 sol) are shown in Fig. 3a for the dried and in Fig. S5 for the calcined samples (Supplementary Materials). The best fit values of the rate constants k_1 obtained for the unmodified and SnO_2-modified TiO_2 catalysts with different SnO_2 loadings are presented in Table S3 (Supplementary Materials), together with the relative photocatalytic activities, calculated with respect to the value of the rate constant k_1 of the unmodified TiO_2 photocatalyst dried at 150 °C. The histogram of the relative photocatalytic activities of the unmodified and SnO_2-modified, dried and calcined, samples is shown in Fig. 3b.

The photocatalysts dried at 150 °C show up to 30% improved relative photocatalytic activities when the TiO_2 is modified with low SnO_2 concentrations (0.1–1 mol.%). The best performing among them is the 0.1SnO_2-TiO_2 sample. When the SnO_2 concentration increases above 1 mol.%, the photocatalytic activity remains in the range of the unmodified TiO_2. Calcination of the samples results in an overall reduced photoactivity. The relative photocatalytic activity of the calcined unmodified TiO_2 is about 30% lower than the photocatalytic activity of the unmodified TiO_2 sample dried at 150 °C. The calcined 0.1SnO_2-TiO_2 sample shows only about 5% lower relative activity. The samples with SnO_2 concentrations above 1 mol.% have 15–20% reduced performance compared to the dried unmodified TiO_2 and remain comparable to the activity of the calcined unmodified TiO_2. The pure SnO_2 catalyst shows an insignificant photocatalytic performance.

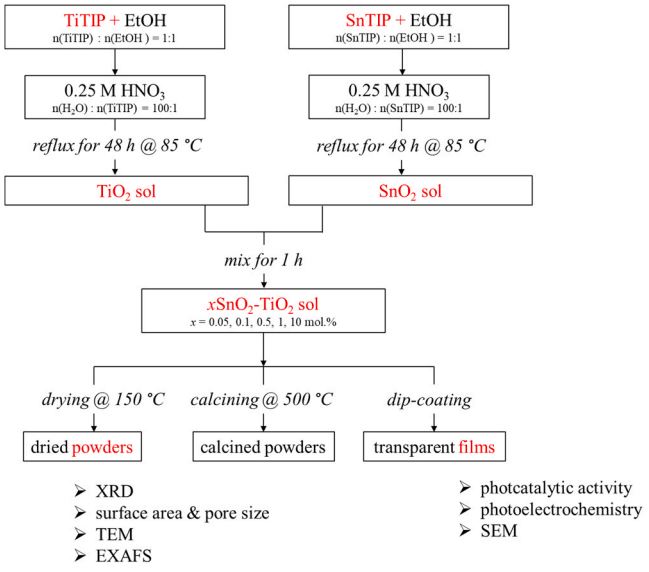

Fig. 2. Schematic diagram of the methodology.

For comparison, the degradation rate of PB in simulated wastewater was tested on the unmodified TiO_2 sample dried at 150 °C. The photoefficiency here is reduced to only 20% of that in deionized water. The result (shown in Fig. 3b) is expected since the wastewater contains other organic molecules that are degraded in the presence of the photocatalyst. Even though the degradation kinetics is slower, this only means that longer exposure times would be required to completely degrade the dye.

Furthermore, the photoefficiency of the prepared photocatalysts is compared with the commercially available Bioclean® glass. The reference glass shows only about 50% of efficiency compared to the unmodified TiO_2 sample dried at 150 °C. This is also to be expected since such a commercial coating with high transparency is primarily used as a self-cleaning glass, where fast kinetics of photocatalytic degradation is not required. In this respect, our thin films, which are also transparent to visible light, show enhanced photoactivity even in aqueous phase.

3.2. Crystalline structure (XRD)

The XRD patterns of the unmodified TiO_2, SnO_2-modified TiO_2 and pure SnO_2 (from SnO_2 sol) powder samples are shown in Fig. 4a for the dried and in Fig. 4b for the calcined photocatalysts. All samples, regardless of the temperature treatment and SnO_2 concentration, show diffraction peaks of crystalline TiO_2 (anatase, brookite and in some cases rutile) and also very broad peaks of crystalline SnO_2 (at high SnO_2 concentrations). The diffractogram peaks of the dried powder catalysts (Fig. 4a) are broad; nevertheless, they are characteristic enough to confirm the formation of crystalline phases despite the treatment at low temperature (150 °C). Calcination (at 500 °C) promotes crystallization and growth of crystallites, which is evident from the sharp and distinct peaks of the diffractograms (Fig. 4b).

The most intense diffraction peaks of (101) anatase, (121) brookite, (110) rutile and (110) cassiterite were used to determine the lattice parameters and relative proportion of each phase, as well as the crystallite sizes (the values are tabulated in Supplementary Materials in Table S5 for the samples dried at 150 °C and in Table S6 for the samples calcined at 500 °C). Within the estimated error bars, the SnO_2 modification of TiO_2 does not affect the size of the crystal unit cell parameters in comparison to the unmodified TiO_2 photocatalyst. The relative amount of each phase depends on the SnO_2 concentration and the temperature treatment of the powders.

The relative amount of each crystalline phase for the unmodified and SnO_2-modified TiO_2 photocatalysts are presented in histograms in Fig. 4c for the dried and Fig. 4d for the calcined samples). Only two crystalline phases of TiO_2 (anatase and brookite) are detected in the dried unmodified and SnO_2-modified samples at low SnO_2 concentrations (0.05–1 mol.%). The analysis shows that there is 70% anatase present, the rest is brookite and no rutile phase is detected. When the SnO_2 concentration is increased above 1 mol.%, the relative amount of the rutile TiO_2 phase increases. This is expected, since Sn is a promoter of the anatase to rutile transformation [8]. When SnO_2 concentration is 10 mol.%, 20% rutile TiO_2 is present in addition to 60% anatase and 20% brookite. There is no crystalline SnO_2 structure detected in the dried SnO_2-modified samples at any of the investigated SnO_2 concentrations up to 10 mol.%.

Calcination of powder catalysts at 500 °C significantly promotes the transformation of the anatase to the thermodynamically stable rutile phase in unmodified and all SnO_2-modified samples. In the calcined unmodified TiO_2 there is 16% rutile. The relative amount of rutile increases up to 85–90% in the samples with low SnO_2 concentrations (0.05–0.5 mol.%). In these samples the anatase phase is still present in 15–10% but the brookite vanishes. In the samples with higher SnO_2 concentration (1 and 10 mol.%) all three crystalline TiO_2 phases are

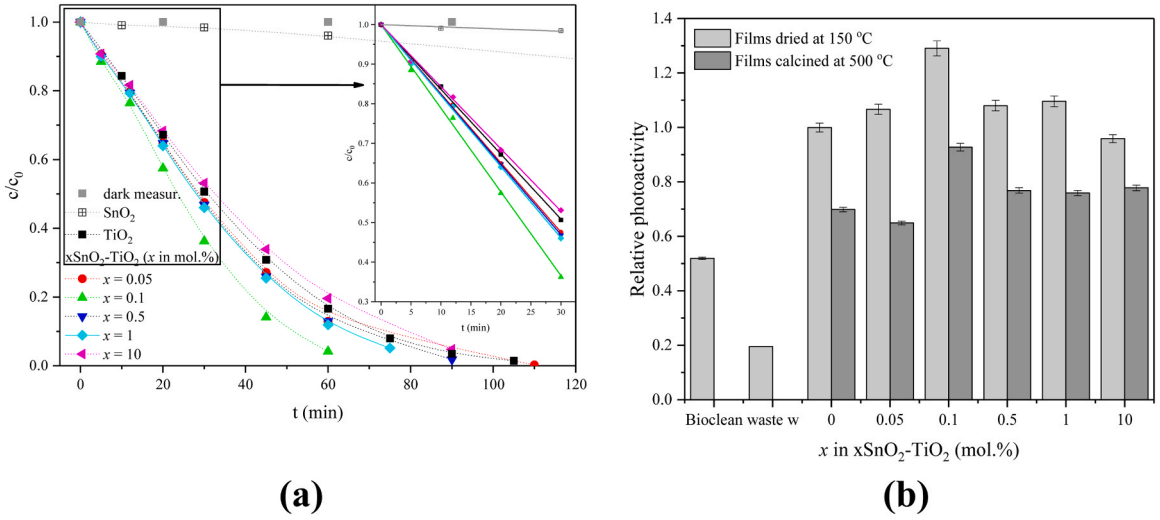

Fig. 3. (a) PB dye concentrations as a function of UV-illumination time for unmodified TiO_2, SnO_2-modified TiO_2 catalysts with different SnO_2 concentrations (0.05–10 mol.%) and pure SnO_2, dried at 150 °C. Insert: Enlarged view of the graphs in the first 30 min of UV-illumination (dots – experiment, solid line – best fit model, $c/c_0 = 1 - k_1 \cdot t$). (b) Histogram of relative photocatalytic activities of unmodified and SnO_2-modified TiO_2 samples dried at 150 °C and calcined at 500 °C. x denotes mol.% of SnO_2 in SnO_2-modified TiO_2 photocatalysts, where x = 0 means unmodified TiO_2. For comparison, the relative photocatalytic activity of the commercial Bioclean® glass and relative photoactivity of unmodified TiO_2 dried at 150 °C in simulated waste water is shown.

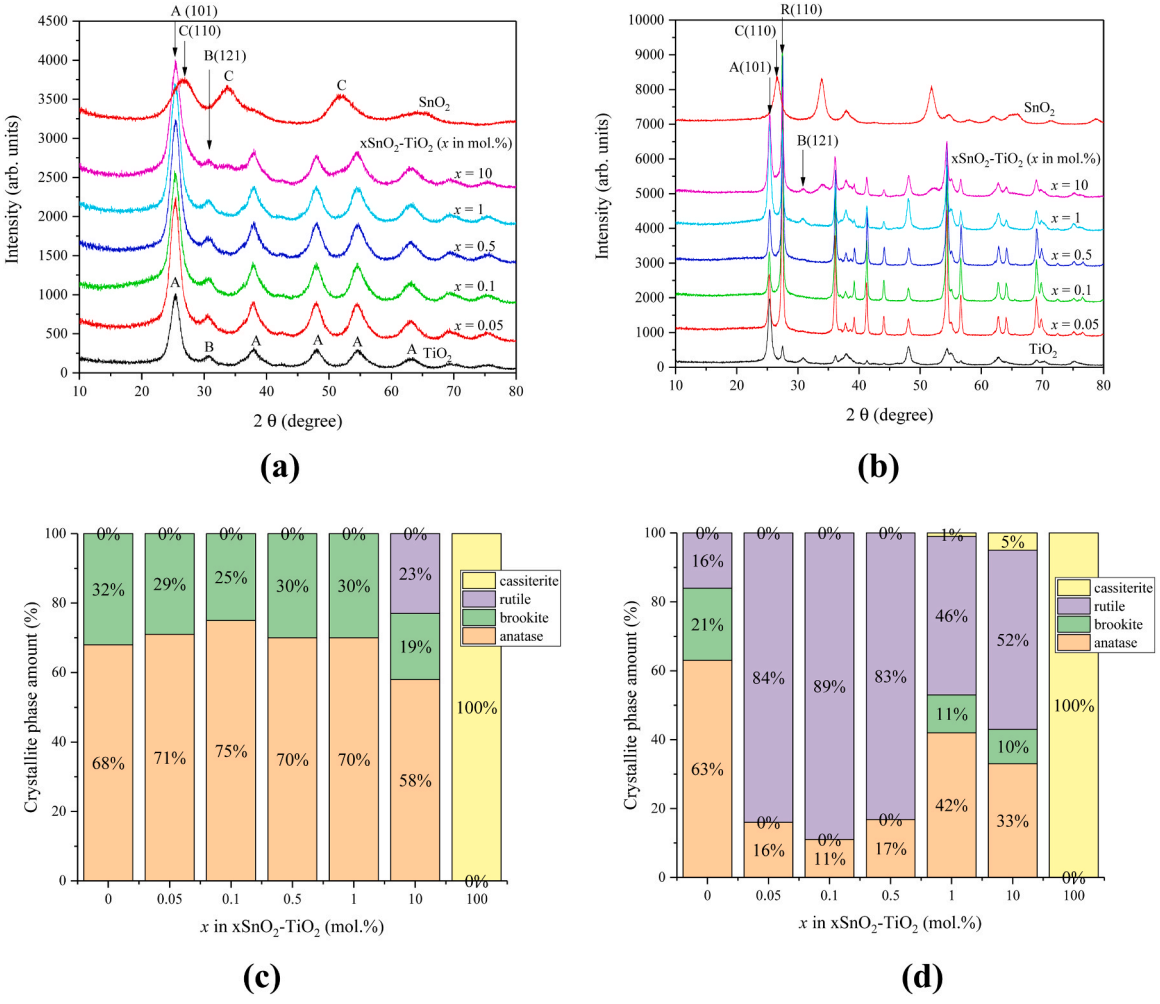

Fig. 4. XRD patterns of unmodified TiO_2 and SnO_2-modified TiO_2 powder photocatalysts dried at 150 °C (a) and calcined at 500 °C (b). Relative amount of anatase (A), brookite (B), rutile (R) and cassiterite (C) crystalline phases in unmodified and SnO_2-modified TiO_2 powder photocatalysts dried at 150 °C (c) and calcined at 500 °C (d). x denotes mol.% of SnO_2 in SnO_2-modified TiO_2 photocatalysts, where x = 0 means unmodified TiO_2 and x = 100 means sample powder obtained from pure SnO_2 sol.

present: rutile (50%), anatase (40%) and brookite (about 10%). In addition, a 1–5% crystalline SnO_2 cassiterite phase is also detected.

The crystallite size values, determined from the width of the diffraction peaks, are summarized in Supplementary Materials in Table S5 for the dried samples and in Table S6 for the calcined ones. The histograms of the crystallite sizes are shown in Supplementary Materials in Fig. S6 for the dried (a) and calcined (b) samples. In the dried powder samples, the size of the anatase crystallites is about 4 nm, brookite 6 nm and rutile 3 nm. After calcination and at the SnO_2 concentration below 0.5 mol.%, the size of the anatase and rutile crystallites grows to about 20 nm and 30 nm, respectively. At higher SnO_2 concentrations (1–10 mol.%), the size of anatase and rutile decreases with increasing SnO_2 concentration. This phenomenon is in the literature known as the growth-retarding effect of the Sn on titania [33–35]. In the $10SnO_2$-TiO_2 sample, the size of the detected cassiterite crystallites is about 6 nm.

A comparison of the XRD data with the photocatalytic properties of the samples shows that the photocatalytic efficiency is reduced by the growth of the crystallite sizes (after calcination of the samples) and by the excessive formation of the rutile crystal phase (in the case of calcined samples and the dried samples with high amount of SnO_2). The XRD results cannot explain the improved activity of the dried SnO_2-modified photocatalysts with low SnO_2 concentrations (0.1–1 mol.%) because no differences in the crystalline structure were detected between them. However, it should be noted that even though no rutile TiO_2 and cassiterite SnO_2 crystallites are detected in these samples, it cannot be excluded that smaller rutile TiO_2 and cassiterite SnO_2 nanoparticles with sizes below the detection limit of XRD are present. To clarify this point, the Sn K-edge EXAFS analysis is used and presented below.

3.3. BET specific surface area

The values of BET surface area and average pore size of the dried and calcined, unmodified and SnO_2-modified TiO_2 samples, are tabulated in Table S7 (Supplementary Materials). A histogram of BET surface area is presented in Fig. 5a and a histogram of average pore sizes in Fig. 5b.

All dried SnO_2-modified samples have approximately the same specific surface area (200 m^2/g) and the average pore size (8 nm) regardless of SnO_2 concentration. Therefore, also these results cannot explain the differences in the photocatalytic activities between them.

However, calcination of the powders results in about 4-times smaller BET specific surface area and about 3-times larger pore sizes in comparison to the dried samples. The smaller BET values of the calcined samples are in agreement with the overall reduced photocatalytic activities compared to the dried samples. But the lowest BET value (2.3 m^2/g) for the calcined $0.1SnO_2$-TiO_2 sample is contradictory to the fact that this sample shows the best photocatalytic performance in the calcined series. Again, this suggests that the BET values cannot explain all the observed differences in the photocatalytic activities between the samples that are equally thermally treated.

The BET results are in agreement with the values of crystallite sizes obtained by XRD: the smaller the BET is, the larger the size of crystallites after calcination. As a result, there are fewer active sites per unit mass in the calcined samples, which partly explains the decrease of photocatalytic activity after calcination.

3.4. Electron micrographs (TEM)

The morphology of the SnO_2-modified photocatalysts (0.5 and 10 mol.% SnO_2) calcined at 500 °C were examined by TEM and HRTEM. At the low SnO_2 concentration (0.5 mol.% SnO_2) there are smaller quasi-round and larger quasi-square shaped TiO_2 crystallites observed (Fig. S7a in Supplementary Materials). The size of the titania nanoparticles, observed by TEM, coincides with the size of the crystallites, observed by XRD. In our case, the sizes of the crystallite domains (determined by XRD) are comparable to the size of the particle sizes (observed by TEM), since we are in the nano size range. The observed anatase nanoparticles are in the size range of 15–20 nm (Fig. S7b in Supplementary Materials), while the observed rutile nanoparticles are found in the size range of 30–40 nm (Fig. S7a in Supplementary Materials). At high SnO_2 concentration (10 mol.%), the anatase and rutile nanoparticles are smaller and are comparable to the crystallite size range of 10–20 nm (Fig. S7c in Supplementary Materials).

A separate phase is observed in the calcined catalysts with 10 mol.% SnO_2. In some cases it can be seen as round droplets among the crystalline titania agglomerates (Fig. 6a). The droplets, which do not display a crystalline structure, are quickly formed (in less than one minute) under electron irradiation during the TEM imaging. In some cases, the droplets were observed to coalesce to form a larger droplet. The instability under the electron beam and the darker contrast (which indicates the drops are composed of heavier atoms than titanium, i.e. Sn) are compatible with the hypothesis that this is SnO_x phase.

The EDX elemental mapping on clusters of $10SnO_2$-TiO_2 photocatalyst calcined at 500 °C (Fig. 6b) shows that there are Sn rich and Sn depleted regions over the titania nanocrystallites. The presence of

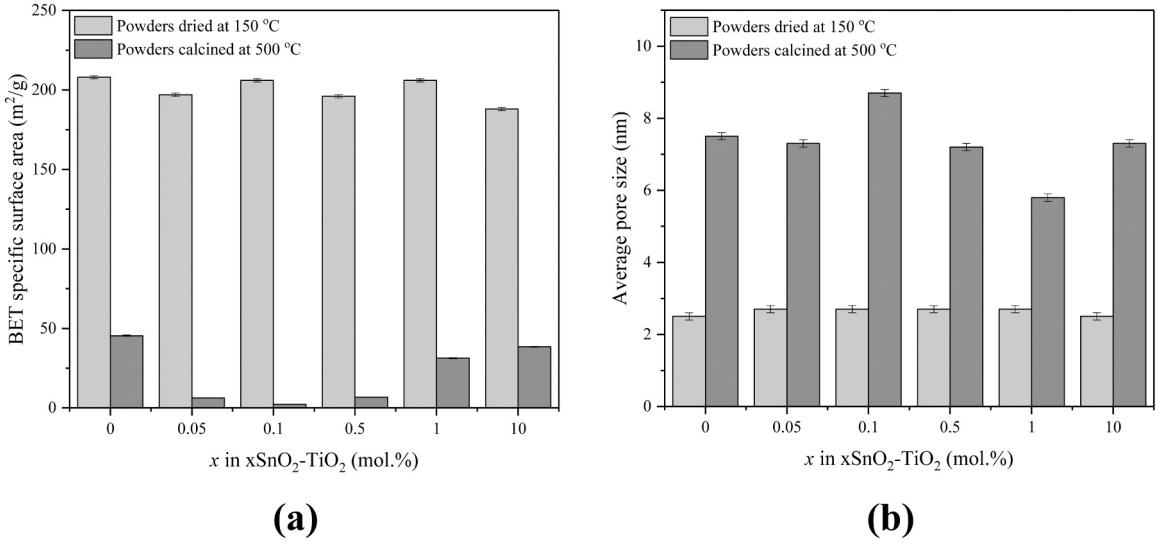

Fig. 5. Histogram of BET specific surface area (a) and average pore size (b) of unmodified and SnO_2-modified TiO_2 samples dried at 150 °C and calcined at 500 °C. x denotes mol.% of Sn in SnO_2-modified TiO_2 photocatalysts, where x = 0 means unmodified TiO_2.

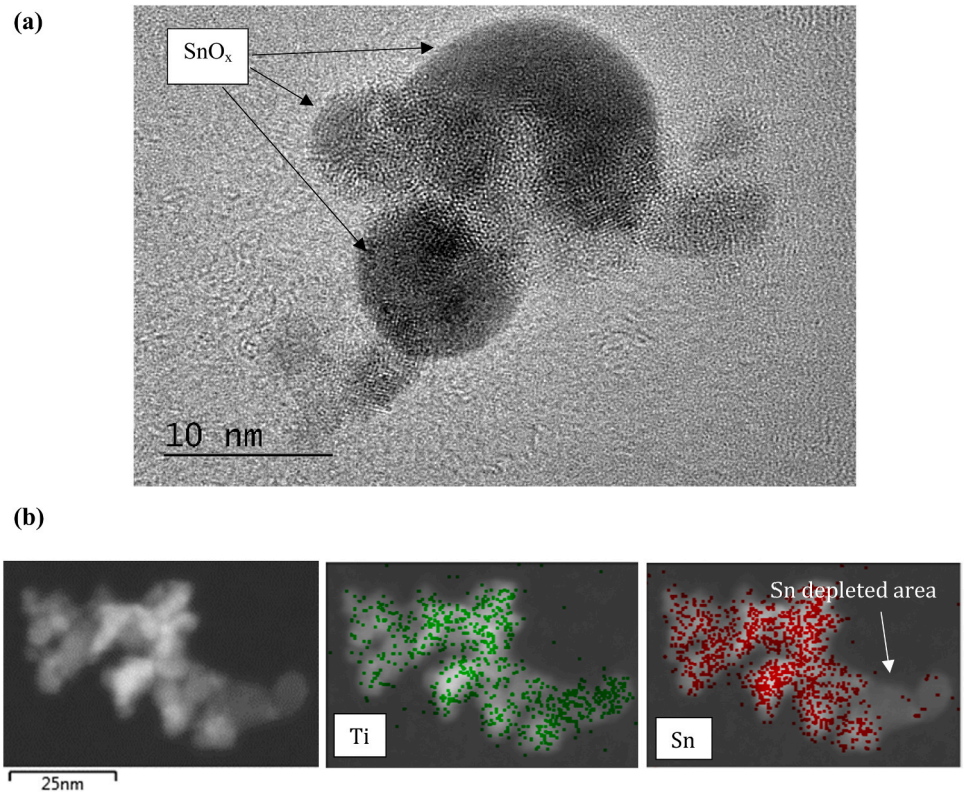

Fig. 6. (a) TEM micrograph of $10SnO_2$-TiO_2 photocatalyst calcined at 500 °C. SnO_x droplets among TiO_2 crystallite are indicated. (b) STEM image and elemental EDX maps of Ti (green) and Sn (red) in $10SnO_2$-TiO_2 photocatalyst calcined at 500 °C. (For interpretation of the references to colour in this figure legend, the reader is referred to the web version of this article.)

regions where the Sn is not detected confirms that Sn is not homogeneously distributed within the titania crystallites, as expected if Sn forms a separate phase.

3.5. Sn K-edge EXAFS

To clearly identify the mechanism responsible for the enhanced or hindered photocatalytic properties in SnO_2-modified TiO_2 photocatalysts and to clarify the role of Sn cations in the photocatalytic process of TiO_2, the structural features below 1 nm had to be recognized. For this purpose, the Sn K-edge EXAFS analysis was used to determine the local structure around the Sn cations and their site of incorporation on the titania nanoparticles in the photocatalysts.

The k^3-weighted Sn K-edge EXAFS spectra of the dried SnO_2-modified TiO_2 photocatalysts (with 0.1, 0.5, 1 and 10 mol.% SnO_2), one additionally calcined sample (with 1 mol.% SnO_2) and the reference SnO_2 are shown in Fig. S8 (in Supplementary Materials) and their Fourier transforms in Fig. 7.

The Fourier transform spectra (Fig. 7) reveal the contributions of consecutive shells of Sn neighbours from 1 Å to about 4 Å. The qualitative comparison of the *FT*-spectra shows no significant structural differences around Sn cations between the samples, regardless of the concentration of SnO_2 and the temperature treatment of the samples. Moreover, the *FT*-spectra of the SnO_2-TiO_2 samples are similar to that of the reference crystalline SnO_2 but with a reduced amplitude of the second and third shell of the neighbour atoms, indicating the presence of SnO_2 nanoparticles with cassiterite structure.

A mixture of two Sn local structures is expected in the SnO_2-modified TiO_2 photocatalysts. Besides Sn local structure typical for the cassiterite, rutile-type SnO_2, some Sn cations can be attached to the surface of titania nanoparticles around them, forming Sn-O-Ti bridges.

The Sn K-edge EXAFS spectra of the SnO_2-modified TiO_2 catalyst samples are modelled with a combined FEFF model, composed of neighbour atoms at distances typical for the expected nanocrystalline cassiterite SnO_2 and Sn atoms attached to the surface of TiO_2 nanoparticles (relative amount of Sn-O-Ti bridges). A detailed description of the two FEFF models and the obtained best fit parameters in EXAFS fits are given in Supplementary Materials.

The EXAFS results show that the rutile-type SnO_2 phase is formed in all SnO_2-modified TiO_2 photocatalysts. The crystalline local SnO_2 structure is already formed in the low-temperature treated catalyst, i.e., after drying at 150 °C (not detectable by XRD). Calcination of the samples at 500 °C does not change the parameters of the crystalline SnO_2 neighbour structure. The first shell of the nearest oxygen neighbours is identical for all samples as described in the bulk SnO_2. The crystal lattice interatomic distances and Debye-Waller factors are the same for all samples regardless of SnO_2 concentration and temperature treatment, in agreement with the rutile-type SnO_2 cassiterite reference structure (Table S8 in Supplementary Materials). However, the coordination numbers of the second and third Sn neighbour shells are for about 50% smaller than expected in the rutile SnO_2 bulk (Table S9), which indicates that nanosized crystalline SnO_2 particles are formed on the surface of the TiO_2 nanoparticle.

Furthermore, the EXAFS results show that the SnO_2 nanoparticles are attached to the TiO_2 phase via Sn-O-Ti bonding. The relative amount of the Sn-O-Ti bridges is the same (10% ± 5%) at all SnO_2 concentrations in all SnO_2-modified TiO_2 photocatalysts dried at 150 °C. The relative amount of the Sn-O-Ti bridges is maintained even after calcination at 500 °C.

The EXAFS results supplement the HRTEM observations, where the SnO_x is observed on the titania surface. Thus, the SnO_2 phase is in the form of small crystalline cassiterite nanoparticles, attached to the surface of the titania nanoparticles, so there are sufficient connections between the TiO_2 and cassiterite SnO_2 nanoparticles at the atomic level.

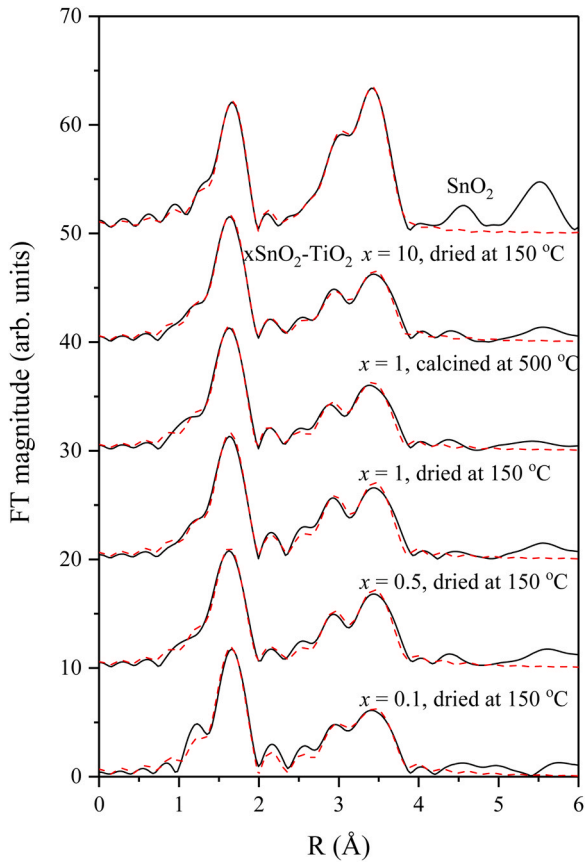

Fig. 7. Fourier transform magnitudes of the k^3-weighted Sn K-edge EXAFS spectra measured on SnO_2-modified TiO_2 photocatalysts dried at 150 °C and calcined sample with 1 mol.% of SnO_2. The spectrum of crystalline SnO_2 (cassiterite) reference is added for comparison. The FT-spectra are calculated in the k-range of 4.5–14.5 $Å^{-1}$ (black solid line – experiment, red dashed line – EXAFS model calculated in the R-range of 1.2–4.0 Å). (For interpretation of the references to colour in this figure legend, the reader is referred to the web version of this article.)

3.6. Photoelectrochemistry

The transient current response measurements, which are shown in Fig. S9a, exhibit an anodic stationary photocurrent, appearing promptly upon switching on the light, with the presence of spikes of the same sign, and then decreasing sharply to finally reach a steady-state value. EIS measurements were performed to investigate the kinetics of charge transfer at the solid-liquid interface, and the data were fitted to the equivalent model as illustrated in Fig. S9b. Mott-Schottky plots (Fig. S9c) were obtained by electrochemical impedance measurements at a constant frequency of 10 kHz. The electronic properties of the dried and calcined $xSnO_2$-TiO_2 thin films were assessed in terms of the flat band potential (E_{FB}) and the donor density (N_D), which can be obtained from the intercept with the x-axis and the slope of the linear part of the plot, respectively (See Eq. S1). The steady-state photocurrent density (J), the semiconductor/electrolyte charge transfer resistance (R_{CT}), the donor density (N_D), and the flat band potential (E_{FB}) values of dried and calcined $xSnO_2$-TiO_2 samples are listed in Table 1.

Results in Table 1 indicate that the addition of SnO_2 does not affect significantly the photoelectrochemical properties of TiO_2. Conversely, the temperature treatment (i.e. dried at 150 °C vs. calcined ta 500 °C) shows a more prominent effect. Samples that have been calcined exhibit significantly higher photocurrent density, lower charge transfer resistance, and more donor states than those that have been dried. This, however, is in contradiction to what has been observed with the photocatalytic activity results. In the case of the dried samples, the contact between the semiconductor and the electrode can be considered the major reason for such performance, while, in the case of calcined samples, it is the % of rutile that plays a more influential role. Higher rutile % in calcined samples leads to an improved water photosplitting process and, consequently, higher photocurrent [36,37]. On the other hand, higher anatase % in the dried samples leads to an improved dye degradation process and, consequently, higher photocatalytic activity in the presence of the targeted dye [38,39]. The higher % of rutile in calcined samples also improves the absorption of visible light. Rutile has a typical band gap value of 3.0 eV (in comparison to 3.2 eV of anatase) and hence is more capable of absorbing visible light. This could explain the higher photocurrent observed for calcined samples in comparison to those that were dried. It is important to note here that the photocatalytic activity runs were performed under pure UV light (centered at 365 nm), while the photoelectrochemical characterizations were done under UV–vis irradiation (centered at 382 nm). In the future, to obtain a better insight into the correlation of both experiments, the conditions should be equalized.

4. Conclusion

The objective of this research was to investigate how the photocatalytic activity of pure TiO_2 can be improved by tin modification. Sn oxide was used to prepare SnO_2-TiO_2 photocatalysts, in contrast to our previous work [8], where Sn-modified TiO_2 photocatalysts were prepared by using Sn cations as promoter of anatase to rutile transformation. In both cases, we have developed a new low-temperature sol-gel synthesis route, based on organic Ti and Sn precursors. In the present case the precursors underwent sol-gel reactions separately to form SnO_2-TiO_2 sol (SnO_2-modified TiO_2), while in the previous case the precursors underwent sol-gel reactions together to form Sn-TiO_2 sol (Sn-modified TiO_2).

The SnO_2-modified TiO_2 sol-gels were deposited on a glass substrate by a dip-coating technique and dried at 150 °C to obtain the photocatalysts in the form of a thin film. To test the thermal stability of the material, an additional set of photocatalysts was prepared by calcining the dried samples in air at 500 °C.

The photocatalytic activity of the air-dried photocatalysts is increased up to 30%, when TiO_2 is modified with low SnO_2 concentrations (0.1–1 mol.%). At higher concentrations, the dried samples show lower photocatalytic activity compared to the unmodified TiO_2 photocatalyst. The results of the BET specific surface area, pore size, crystal size and crystal lattice parameters show no distinct features to explain the differences between the activities of the dried samples. The main

Table 1
Photoelectrochemical properties of dried and calcined $xSnO_2$-TiO_2 samples. N_D and E_{FB} values for calcined 0.1% SnO_2-TiO_2 were not computed due to possible contamination or poor film/substrate adhesion.

Sample	J [μA/cm^2] Dried at 150 °C	R_{CT} [kΩ/cm^2]	N_D x10^{19} [cm^{-3}]	E_{FB} [V vs. Ag/AgCl]	J [μA/cm^2] Calcined at 500 °C	R_{CT} [kΩ/cm^2]	N_D x10^{19} [cm^{-3}]	E_{FB} [V vs. Ag/AgCl]
TiO_2	0.9	44.8	9.8	-0.53	1.0	17.2	23.3	-0.60
$xSnO_2$-TiO_2 x [mol.%]								
0.1	0.8	48.4	6.5	-0.53	1.5	15.3	–	–
10	0.3	34.8	7.5	-0.54	1.8	16.1	16.7	-0.47

difference between them is the crystalline structure. EXAFS results show that nanostructured cassiterite SnO_2 is formed already in the low-temperature treated samples. The SnO_2 nanoparticles are directly connected to the surface of TiO_2 nanocrystallites via the Sn-O-Ti bonding. In this way a coupled system of two semiconductors SnO_2-TiO_2 is formed. An optimal ratio and a sufficient contact of the two phases is achieved in the low SnO_2 concentration range (0.1–1 mol.%), and consequently these samples are the most photocatalytically active. The synergy of the two semiconductors has a beneficial effect on the increased lifetime of the photogenerated electrons and holes through an effective charge carrier separation. The mechanism of improved photoactivity is analogous to that we found in the Sn-modified TiO_2 [8], where in a same way a coupled system of two semiconductors (anatase-rutile TiO_2) facilitates charge separation and enhances the photocatalytic efficiency of titania coatings.

Calcination at 500 °C of the SnO_2-modified TiO_2 photocatalysts induces significant structural changes: the titania nanocrystals grow, have a smaller specific surface area and a larger average pore size, resulting in an overall reduced activity compared to the samples dried at 150 °C. In addition, the calcination promotes the transformation of the anatase to the thermodynamically stable rutile phase. The relative amount of the rutile TiO_2 phase increases significantly in all photocatalysts with different SnO_2 concentrations. As a result, the photocatalytic activity is greatly reduced because under UV irradiation the rutile has a lower photocatalytic efficiency in comparison to the anatase. Higher SnO_2 concentration increases the amount of the cassiterite SnO_2 nanoparticles located on and/or adjacent to the TiO_2 nanocrystals. The amount of cassiterite nanoparticles, effectively bonded to the titania nanoparticles, remain unchanged, therefore the photo-efficiency remains almost at the level of the calcined unmodified TiO_2, since the SnO_2 per se does not show photocatalytic activity. It might be expected that significantly higher amounts of the SnO_2 modifier (20–50%) would lead to an obviously hindered photocatalytic activity due to a shielding effect of the cassiterite, covering titania nanoparticles. Moreover, it will be interesting to test the SnO_2-modified TiO_2 photocatalysts also for the efficiency to other contaminants of emerging concern (i.e., pharmaceutical pollutants, such as antibiotics, etc.).

CRediT authorship contribution statement

Ksenija Maver: Conceptualization, analysis, Investigation, Writing - original draft, Writing – review & editing. **Iztok Arčon:** Conceptualization, analysis, Investigation, Writing – review & editing. **Matta Fanetti:** Investigation, Writing - review & editing. **Samar Al Jitan:** Investigation, Writing - review & editing. **Giovanni Palmisano:** Investigation, Writing - review & editing. **Matjaž Valant:** Supervision. **Urška Lavrenčič Štangar:** Conceptualization, Writing - review & editing, Funding acquisition.

Declaration of Competing Interest

The authors declare that they have no known competing financial interests or personal relationships that could have appeared to influence the work reported in this paper.

Acknowledgements

We acknowledge access to SR facility at DESY, beamline P65 of PETRA III, Hamburg (project I-20170160 EC). We would like to thank Edmund Welter of PETRA III for expert advice on beamline operation. This research was supported by the Slovenian Research Agency (P1-0112, L2-7630, L7-1848 and P1-0134), and by the project CALIPSOplus under the Grant Agreement 730872 from the EU Framework Programme for Research and Innovation HORIZON 2020, EU. The authors also kindly acknowledge Mojca Opresnik from the National Institute of Chemistry for BET measurements and dr. Boštjan Žener from the University of Ljubljana, Faculty of Chemistry and Chemical Technology, for SEM measurements.

Appendix A. Supporting information

Supplementary data associated with this article can be found in the online version at doi:10.1016/j.cattod.2021.06.018.

References

[1] T. Oppenländer, Photochemical Purification of Water and Air: Advanced Oxidation Processes (AOPs) - Principles, Reaction Mechanisms. Reactor Concepts, Wiley, 2007.
[2] J. Coronado, F. Fresno, M. Hernández-Alonso, R. Portela, S. Suárez, S. García Rodríguez, V. de la Peña O'Shea, Design of Advanced Photocatalytic Materials for Energy and Environmental Applications, 2013. ⟨https://doi.org/10.1007/978-1-4471-5061-9⟩.
[3] M.R.D. Khaki, M.S. Shafeeyan, A.A.A. Raman, W.M.A.W. Daud, Application of doped photocatalysts for organic pollutant degradation - a review, J. Environ. Manag. 198 (2017) 78–94, https://doi.org/10.1016/j.jenvman.2017.04.099.
[4] V. Kumaravel, S. Mathew, J. Bartlett, S.C. Pillai, Photocatalytic hydrogen production using metal doped TiO_2: a review of recent advances, Appl. Catal. B Environ. 244 (2019) 1021–1064, https://doi.org/10.1016/j.apcatb.2018.11.080.
[5] N. Yuangpho, S.T.T. Le, T. Treerujiraphapong, W. Khanitchaidecha, A. Nakaruk, Enhanced photocatalytic performance of TiO_2 particles via effect of anatase–rutile ratio, Phys. E Low. Dimens. Syst. Nanostruct. 67 (2015) 18–22, https://doi.org/10.1016/j.physe.2014.11.006.
[6] D.C. Hurum, A.G. Agrios, K.A. Gray, T. Rajh, M.C. Thurnauer, Explaining the enhanced photocatalytic activity of Degussa P25 mixed-phase TiO_2 using EPR, J. Phys. Chem. B 107 (2003) 4545–4549, https://doi.org/10.1021/jp0273934.
[7] D.A.H. Hanaor, C.C. Sorrell, Review of the anatase to rutile phase transformation, J. Mater. Sci. 46 (2011) 855–874, https://doi.org/10.1007/s10853-010-5113-0.
[8] K. Maver, I. Arčon, M. Fanetti, S. Emin, M. Valant, U. Lavrenčič Štangar, Improved photocatalytic activity of anatase-rutile nanocomposites induced by low-temperature sol-gel Sn-modification of TiO_2, Catal. Today 361 (2021) 124–129, https://doi.org/10.1016/j.cattod.2020.01.045.
[9] S. Mahanty, S. Roy, S. Sen, Effect of Sn doping on the structural and optical properties of sol-gel TiO_2 thin films, J. Cryst. Growth 261 (2004) 77–81, https://doi.org/10.1016/j.jcrysgro.2003.09.023.
[10] M.F. Gálvez-López, M.J. Muñoz-Batista, C.G. Alvarado-Beltrán, J.L. Almaral-Sánchez, B. Bachiller-Baeza, A. Kubacka, M. Fernández-García, Sn modification of TiO_2 anatase and rutile type phases: 2-Propanol photo-oxidation under UV and visible light, Appl. Catal. B Environ. 228 (2018) 130–141, https://doi.org/10.1016/j.apcatb.2018.01.075.
[11] F. Fresno, D. Tudela, J.M. Coronado, J. Soria, Synthesis of $Ti_{1-x}Sn_xO_2$ nanosized photocatalysts in reverse microemulsions, Catal. Today 143 (2009) 230–236, https://doi.org/10.1016/j.cattod.2008.10.024.
[12] Y. Yang, H. Li, H. Zhao, R. Qu, S. Zhang, W. Hu, X. Yu, X. Zhu, S. Liu, C. Zheng, X. Gao, Structure and crystal phase transition effect of Sn doping on anatase TiO_2 for dichloromethane decomposition, J. Hazard. Mater. 371 (2019) 156–164, https://doi.org/10.1016/j.jhazmat.2019.02.103.
[13] H. Tada, A. Hattori, Y. Tokihisa, K. Imai, N. Tohge, S. Ito, A patterned-TiO_2/SnO_2 bilayer type photocatalyst, J. Phys. Chem. B 104 (2000) 4585–4587, https://doi.org/10.1021/jp000049r.
[14] K. Awa, R. Akashi, A. Akita, S. ichi Naya, H. Kobayashi, H. Tada, Highly efficient and selective oxidation of ethanol to acetaldehyde by a hybrid photocatalyst consisting of SnO_2 nanorod and rutile TiO_2 with heteroepitaxial junction, Chem. Phys. Chem. 20 (2019) 2155–2161, https://doi.org/10.1002/cphc.201900632.
[15] W. Sangchay, The self-cleaning and photocatalytic properties of TiO_2 doped with SnO_2 thin films preparation by sol-gel method, Energy Procedia 89 (2016) 170–176, https://doi.org/10.1016/j.egypro.2016.05.023.
[16] A. Kusior, L. Zych, K. Zakrzewska, M. Radecka, Photocatalytic activity of TiO_2/SnO_2 nanostructures with controlled dimensionality/complexity, Appl. Surf. Sci. 471 (2019) 973–985, https://doi.org/10.1016/j.apsusc.2018.11.226.
[17] A. Marzec, M. Radecka, W. Maziarz, A. Kusior, Z. Pedzich, Structural, optical and electrical properties of nanocrystalline TiO_2, SnO_2 and their composites obtained by the sol-gel method, J. Eur. Ceram. Soc. 36 (2016) 2981–2989, https://doi.org/10.1016/j.jeurceramsoc.2015.12.046.
[18] A. Regoutz, F.E. Oropeza, C.G. Poll, D.J. Payne, R.G. Palgrave, G. Panaccione, F. Borgatti, S. Agrestini, Y. Utsumi, K.D. Tsuei, Y.F. Liao, G.W. Watson, R.G. Egdell, Identification of metal s states in Sn-doped anatase by polarisation dependent hard X-ray photoelectron spectroscopy, Chem. Phys. Lett. 647 (2016) 59–63, https://doi.org/10.1016/j.cplett.2016.01.013.
[19] I. Rangel-Vázquez, G. Del Angel, V. Bertin, F. González, A. Vázquez-Zavala, A. Arrieta, J.M. Padilla, A. Barrera, E. Ramos-Ramirez, Synthesis and characterization of Sn doped TiO_2 photocatalysts: effect of Sn concentration on the textural properties and on the photocatalytic degradation of 2,4-dichlorophenoxyacetic acid, J. Alloy. Compd. 643 (2015) S144–S149, https://doi.org/10.1016/j.jallcom.2014.12.065.
[20] K. Majrik, E. Tálas, Z. Pászti, I. Sajó, J. Mihály, L. Korecz, E. Drotár, A. Tompos, Enhanced activity of sol-gel prepared SnO_x-TiO_2 in photocatalytic methanol reforming, Appl. Catal. A Gen. 466 (2013) 169–178, https://doi.org/10.1016/j.apcata.2013.06.047.

[21] B. Žener, Ž. Medoš, M.B. Rogač, R.C. Korošec, Monitoring photocatalytic degradation of plasmocorinth B with titania thin films using non-spectroscopic methods, Chem. Sel. 4 (2019) 4112–4117, https://doi.org/10.1002/slct.201900188.
[22] J.D. Ingle, S.R. Crouch, Spectrochemical Analysis, Prentice-Hall, Englewood Cliffs, N.J, 1988.
[23] H. Lachheb, E. Puzenat, A. Houas, M. Ksibi, E. Elaloui, C. Guillard, J.-M. Herrmann, Photocatalytic degradation of various types of dyes (Alizarin S, Crocein Orange G, Methyl Red, Congo Red, Methylene Blue) in water by UV-irradiated titania, Appl. Catal. B Environ. 39 (2002) 75–90, https://doi.org/10.1016/S0926-3373(02)00078-4.
[24] U. Černigoj, U.L. Štangar, P. Trebše, U.O. Krašovec, S. Gross, Photocatalytically active TiO_2 thin films produced by surfactant-assisted sol-gel processing, Thin Solid Films 495 (2006) 327–332, https://doi.org/10.1016/j.tsf.2005.08.240.
[25] T. Degen, M. Sadki, E. Bron, U. König, G. Nénert, The HighScore suite, Powder Diffr 29 (2014) S13–S18, https://doi.org/10.1017/S0885715614000840.
[26] A.L. Patterson, The Scherrer formula for X-ray particle size determination, Phys. Rev. 56 (1939) 978–982, https://doi.org/10.1103/PhysRev.56.978.
[27] S. Brunauer, P.H. Emmett, E. Teller, Adsorption of gases in multimolecular layers, J. Am. Chem. Soc. 60 (1938) 309–319, https://doi.org/10.1021/ja01269a023.
[28] E.P. Barrett, L.G. Joyner, P.P. Halenda, The determination of pore volume and area sistributions in porous substances. I. Computations from nitrogen isotherms, J. Am. Chem. Soc. 73 (1951) 373–380, https://doi.org/10.1021/ja01145a126.
[29] C.A. Schneider, W.S. Rasband, K.W. Eliceiri, NIH Image to ImageJ: 25 years of image analysis, Nat. Methods 9 (2012) 671–675, https://doi.org/10.1038/nmeth.2089.
[30] B. Ravel, M. Newville, ATHENA, ARTEMIS, HEPHAESTUS: data analysis for X-ray absorption spectroscopy using IFEFFIT, J. Synchrotron Radiat. 12 (2005) 537–541, https://doi.org/10.1107/S0909049505012719.
[31] J.J. Rehr, R.C. Albers, S.I. Zabinsky, High-order multiple-scattering calculations of X-ray-absorption fine structure, Phys. Rev. Lett. 69 (1992) 3397–3400, https://doi.org/10.1103/PhysRevLett.69.3397.
[32] C. Garlisi, C.-Y. Lai, L. George, M. Chiesa, G. Palmisano, Relating photoelectrochemistry and wettability of sputtered Cu- and N-doped TiO_2 thin films via an integrated approach, J. Phys. Chem. C 122 (2018) 12369–12376, https://doi.org/10.1021/acs.jpcc.8b03650.
[33] J. Wallot, P. Reynders, A.A. Herzing, C.J. Kiely, M.P. Harmer, J. Rödel, Sintering of thin film nanocrystalline titania-tin oxide composites, J. Eur. Ceram. Soc. 28 (2008) 2225–2232, https://doi.org/10.1016/j.jeurceramsoc.2008.02.019.
[34] Z.M. Shi, L. Yan, L.N. Jin, X.M. Lu, G. Zhao, The phase transformation behaviors of Sn^{2+}-doped titania gels, J. Non Cryst. Solids 353 (2007) 2171–2178, https://doi.org/10.1016/j.jnoncrysol.2007.02.048.
[35] K.N.P. Kumar, D.J. Fray, J. Nair, F. Mizukami, T. Okubo, Enhanced anatase-to-rutile phase transformation without exaggerated particle growth in nanostructured titania-tin oxide composites, Scr. Mater. 57 (2007) 771–774, https://doi.org/10.1016/j.scriptamat.2007.06.039.
[36] A. Miyoshi, S. Nishioka, K. Maeda, Water splitting on rutile $TiO_{(2)}$ -based photocatalysts, Chemistry 24 (2018) 18204–18219, https://doi.org/10.1002/chem.201800799.
[37] E. Pulido Melián, O. González Díaz, A. Ortega Méndez, C.R. López, M. Nereida Suárez, J.M. Doña Rodríguez, J.A. Navío, D. Fernández Hevia, J. Pérez Peña, Efficient and affordable hydrogen production by water photo-splitting using TiO_2-based photocatalysts, Int. J. Hydrog. Energy 38 (2013) 2144–2155, https://doi.org/10.1016/j.ijhydene.2012.12.005.
[38] M. Xie, L. Jing, J. Zhou, J. Lin, H. Fu, Synthesis of nanocrystalline anatase TiO_2 by one-pot two-phase separated hydrolysis-solvothermal processes and its high activity for photocatalytic degradation of rhodamine B, J. Hazard. Mater. 176 (2010) 139–145, https://doi.org/10.1016/j.jhazmat.2009.11.008.
[39] S.C. Pillai, P. Periyat, R. George, D.E. McCormack, M.K. Seery, H. Hayden, J. Colreavy, D. Corr, S.J. Hinder, Synthesis of high-temperature stable anatase TiO_2 photocatalyst, J. Phys. Chem. C 111 (2007) 1605–1611, https://doi.org/10.1021/jp065933h.